

Using the Evolution of Clusters to Constrain Ω

Vincent R. Eke^{1,2}, Shaun Cole^{1,3} and Carlos S. Frenk^{1,4}

¹*Department of Physics, University of Durham, Science Laboratories, South Rd, Durham DH1 3LE*

²*V.R.Eke@durham.ac.uk*

³*Shaun.Cole@durham.ac.uk*

⁴*C.S.Frenk@durham.ac.uk*

13 November 2018

ABSTRACT

The population of rich galaxy clusters evolves much more rapidly in a universe with critical density than in a universe with low density. Thus, counts of clusters at intermediate redshift offer the possibility of determining the cosmological density parameter, Ω_0 , with a minimum of assumptions. We quantify this evolution using the Press-Schechter formalism which we extend to flat cosmological models with a cosmological constant, $\Lambda_0 = 1 - \Omega_0$. Using new large N-body simulations, we verify that this formalism accurately predicts the abundance of rich clusters as a function of redshift in various cosmologies. We normalise the models by comparing them to the local abundance of clusters as a function of their X-ray temperature which we rederive from data compiled by Henry & Arnaud. The resulting values of the *rms* density fluctuation in spheres of radius $8h^{-1}\text{Mpc}$ are $\sigma_8 = (0.50 \pm 0.04)\Omega_0^{-0.47+0.10\Omega_0}$ if $\Lambda_0 = 0$ and $\sigma_8 = (0.50 \pm 0.04)\Omega_0^{-0.53+0.13\Omega_0}$ if $\Lambda_0 = 1 - \Omega_0$. These values depend only weakly, and almost not at all if $\Omega_0 = 1$, on the shape of the power spectrum. We then examine how the distributions of mass, X-ray temperature and Sunyaev-Zel'dovich decrement evolve as a function of Ω_0 . We present the expected distributions at $z = 0.33$ and $z = 0.5$ and the predicted number counts of the largest clusters, both in space and in projection on the sky. We find that even at $z = 0.33$, these distributions depend very strongly on Ω_0 and only weakly on Λ_0 . For example, at this redshift, we expect 20 times as many clusters per comoving volume with $M > 3.5 \times 10^{14}h^{-1}M_\odot$ and 5 times as many clusters with $kT > 5$ keV if $\Omega_0 = 0.3$ than if $\Omega_0 = 1$. The splitting in the integrated counts is enhanced by the larger volume element in low Ω_0 models. There is therefore a real prospect of estimating Ω_0 from forthcoming surveys of intermediate redshift clusters that will determine their masses, X-ray temperatures or Sunyaev-Zel'dovich decrements.

Key words: galaxies: clusters – cosmology: theory .

1 INTRODUCTION

Galaxy clusters are exceptionally useful tools for estimating fundamental cosmological parameters. Their utility stems largely from their relative dynamical youth. In hierarchical clustering theories, clusters form by the gravitational amplification of primordial density fluctuations, usually assumed to have an initially Gaussian distribution of amplitudes. Rich clusters correspond to the rarest collapsed objects in this distribution and their abundance varies very rapidly with properties such as mass or potential well depth.

The mass within the virial radius of a rich cluster ($\sim 5 \times 10^{14}h^{-1}M_\odot$) is very close to the mass enclosed within a sphere of radius $8h^{-1}\text{Mpc}$ in the unperturbed universe (Evrard 1989, White, Efstathiou & Frenk 1993). Because

of this, the present day abundance of rich clusters directly reflects the amplitude of density fluctuations on a scale of $\sim 8h^{-1}\text{Mpc}$ and can be used to measure this amplitude with a minimum of assumptions. In general, this measure depends only weakly on the amplitude of fluctuations on other scales. It does, however, depend on the value of the cosmological density parameter, Ω_0 . Thus, the observed local cluster abundance fixes the value of σ_8 , the *rms* density fluctuation in spheres of radius $8h^{-1}\text{Mpc}$, as a function of Ω_0 .

The temporal *evolution* of the cluster abundance is determined by the rate at which density perturbations grow. This, in turn, depends primarily on the value of Ω and, to

a lesser extent, the value of the cosmological constant, Λ^* , and the shape of the power spectrum of density fluctuations. In a low density universe, fluctuations cease to grow after a redshift $z \sim (\Omega_0^{-1} - 1)^{-1}$ (e.g. Peebles 1980), resulting in a cluster population that evolves very slowly at low redshift. In an $\Omega_0 = 1$ universe, on the other hand, density fluctuations continue to grow even at the present epoch and so the cluster population is still evolving rapidly. Measurement of the cluster abundance at moderate redshifts provides a powerful method for estimating Ω_0 .

In order to apply these tests, it is necessary to predict and measure the abundance of clusters as a function of some property such as mass, X-ray luminosity or the equilibrium temperature of the X-ray emitting intracluster gas. Theoretical predictions and observational measurements are subject to different uncertainties. The cluster mass within the virial radius is the simplest quantity to predict theoretically, but one of the hardest to measure reliably. Traditional virial analyses are prone to contamination by projection effects (Frenk *et al.* 1990; Van Haarlem, Frenk & White 1996; Mazure *et al.* 1995) and X-ray data do not generally extend to the virial radius. A novel and highly promising technique to measure cluster masses employs the shape distortions of background galaxies produced by weak gravitational lensing in the cluster potential (Kaiser & Squires 1993, Fahlman *et al.* 1994, Wilson, Cole & Frenk 1996, Seitz & Schneider 1995 and references therein.) The limited field of view of the current generation of CCD cameras, however, restricts such measurements to the inner parts of clusters.

The simplest quantity to measure empirically is the cluster X-ray luminosity. However, since the bremsstrahlung emissivity per unit volume is proportional to the square of the gas density, the total power radiated is very sensitively dependent upon the distribution of gas in the cluster core. This is difficult to model, particularly at high redshift (Evrard 1990; Navarro, Frenk & White 1995 and references therein). Nevertheless, X-ray luminosity provides a convenient means to select complete samples of galaxy clusters. In contrast, the temperature of the intracluster gas can be predicted quite reliably using modern hydrodynamic simulations. These show that as a cluster collapses, the gas is shock heated to the virial temperature and rapidly settles into hydrostatic equilibrium with an approximate isothermal structure (Evrard 1990, Cen & Ostriker 1994, Bryan *et al.* 1994, Navarro *et al.* 1995). Average (luminosity-weighted) X-ray temperatures have now been measured for fairly large samples of clusters, with the Einstein Observatory (Henry & Arnaud 1991), and EXOSAT (Edge 1988), and the radial variation of temperature is now beginning to be probed with ASCA (Markevitch *et al.* 1996). Early results show that the gas is indeed approximately isothermal. Finally, another observable that is also insensitive to the detailed distribution of the gas within the cluster is the $\Delta T/T$ decrement in the cosmic microwave background radiation produced by the Sunyaev-Zel'dovich (S-Z) effect (Sunyaev & Zeldovich 1972). The line-of-sight decrement from the cluster depends only on the product of the column density of gas and the temperature and is independent of the cluster redshift. Sunyaev-

Zel'dovich decrements have now been reliably measured for several clusters (eg Grainge *et al.* (1993), Wilbanks *et al.* (1994) and Birkinshaw & Hughes (1994)).

In this paper, we exploit those cluster properties which are best determined theoretically and observationally in order to constrain the values of cosmological parameters. We first use the distribution of X-ray temperatures at the *present day* to estimate σ_8 . We then examine the *evolution* of cluster properties to constrain the value of Ω_0 . Specifically, we present predictions for the mass function, the temperature function and the distribution of S-Z decrements at $z \simeq 0.3 - 0.5$. This range of redshifts is a rich area of observational work. Ongoing programmes include mass measurements from weak gravitational lensing using HST and large format CCDs (Ellis, private communication; Kaiser, private communication); estimates of the cluster temperature function (Henry, private communication); and S-Z source counts and redshift distributions from ground-based radio telescopes and, if approved, from the COBRA-SAMBA satellite mission.

Related calculations have been carried out by Evrard (1989), Frenk *et al.* (1990), Bond & Myers (1992), Lilje (1992), Oukbir & Blanchard (1992), Bahcall & Cen (1993), Hanami (1993), White *et al.* (1993), Bartlett & Silk (1993,1994), Barbosa *et al.* (1995), Hattori & Matsuzawa (1995), Viana & Liddle (1995), amongst others. Our work differs from these earlier studies in various respects. Firstly, we consider a wider range of cosmological models than most previous analyses, particularly models with low values of Ω_0 , with and without a cosmological constant. Secondly, we use some of the largest N-body simulations ever carried out in order to verify the accuracy of our analytical calculations. Finally, we place special emphasis on making detailed predictions in a manner that can be compared to observational data with a minimum of assumptions. Since high-redshift data are not yet sufficiently complete, we do not attempt to estimate Ω_0 in this paper, but present instead a number of distributions that will enable this estimate to be made as the data become available.

This paper is structured as follows. Section 2 reviews the Press-Schechter model for the abundance of clusters, extended to open and flat cosmological models ($\Omega_0 < 1$ with $\Lambda_0 = 0$ or $\Lambda_0 = 1 - \Omega_0$). The predictions of this model are compared with a set of 192^3 particle N-body simulations in Section 3. In Section 4 we review the existing cluster abundance data and normalise the analytical models using the cumulative cluster temperature function estimated from the data compiled by Henry & Arnaud (1991). The evolution of the cluster mass and temperature functions, the S-Z source counts and the dependence of these quantities on Ω_0 and Λ_0 are predicted in Sections 5.1 - 5.3. Finally, we discuss the importance and implications of these results in Section 6.

2 MODEL

An analytical expression for the comoving number density of dark matter halos of mass M in the interval dM , originally derived by Press & Schechter (1974) (see also Bond *et al.* 1991), is

* We express Λ in units of $3H_0^2$, where $H_0 = 100\text{hkm s}^{-1}\text{Mpc}^{-1}$ is the present value of the Hubble constant

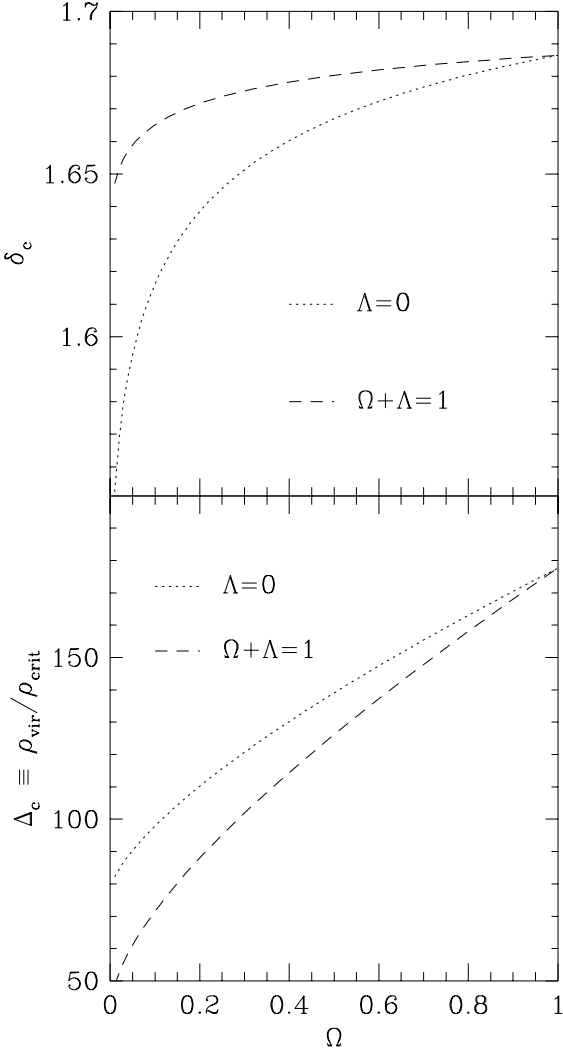


Figure 1. *Upper panel:* critical threshold for collapse, δ_c , as a function of Ω , in the spherical collapse model. Results are plotted for open models with $\Lambda = 0$ (dotted line) and flat models with $\Omega + \Lambda = 1$ (dashed lines). *Lower panel:* the virial density of collapsed objects in units of the critical density. The dotted and dashed lines are as in the upper panel.

$$\frac{dn}{dM} = \left(\frac{2}{\pi}\right)^{\frac{1}{2}} \frac{\bar{\rho}}{M^2} \frac{\delta_c(z)}{\sigma} \left| \frac{d \ln \sigma}{d \ln M} \right| \exp \left[-\frac{\delta_c(z)^2}{2\sigma^2} \right], \quad (2.1)$$

where $\bar{\rho}$ is the present mean density of the universe, and $\sigma(M)$ the present, linear theory *rms* density fluctuation in spheres containing a mean mass M . The evolution with redshift is controlled by the redshift dependent density threshold $\delta_c(z)$. For the case of $\Omega_0 = 1$, the conventional choice of this threshold is $\delta_c(z) = 1.686(1+z)$. This is the value, extrapolated to the present using linear theory, of the overdensity of a uniform spherical overdense region at the point at which the exact non-linear model predicts that it should collapse to a singularity. This threshold, along with the choice of top-hat filtering to define $\sigma(M)$, gives a mass function that agrees remarkably well with the results of N-body simulations (e.g. Efstathiou *et al.* 1985, Lacey & Cole 1994). For $\Omega \neq 1$ one can use the spherical collapse model to derive a

general expression for the density threshold. Expressing the threshold as $\delta_c(z) = \delta_c(0)/D(z, \Omega_0, \Lambda_0)$ where $D(z, \Omega_0, \Lambda_0)$ is the linear growth factor normalised to unity at $z = 0$ (Peebles 1980), we find that $\delta_c(0)$ has only a weak dependence on Ω for both open models with $\Lambda = 0$ and flat models with $\Omega + \Lambda = 1$ (see Fig 1). The details of the $\Lambda = 0$ calculation can be found in Lacey & Cole (1993; see also Maoz 1990), and the $\Omega + \Lambda = 1$ result is derived here in the Appendix (see also Lilje 1992, White *et al.* 1993 and Kochanek 1995).

In order to convert the mass function obtained from (2.1) to a temperature function we assume that the gas is isothermal. In this case,

$$kT_{\text{gas}} = \frac{9.37}{\beta(5X+3)} \left(\frac{M}{10^{15} h^{-1} M_{\odot}} \right)^{\frac{2}{3}} \times (1+z) \left(\frac{\Omega_0}{\Omega(z)} \right)^{\frac{1}{3}} \Delta_c^{\frac{1}{3}} \text{ keV}, \quad (2.2)$$

where Δ_c is the ratio of the mean halo density, to the critical density at that redshift, β is the ratio of specific galaxy kinetic energy to specific gas thermal energy and X is the hydrogen mass fraction which we take to be $X = 0.76$. Recent work by Navarro *et al.* (1995) shows that equation (2.2) is accurately obeyed in N-body/hydrodynamic simulations of the formation of clusters in universes with $\Omega_0 = 1$. Their simulations predict an X-ray luminosity-weighted $\beta = 1.07 \pm 0.05$ for individual clusters, in fair agreement with observational determinations (e.g. Forman & Jones 1990). We adopt the value $\beta = 1$ throughout this paper, but our results may be modified for different choices simply by rescaling all predicted temperatures by β^{-1} .

The density contrast Δ_c is computed from the spherical collapse model assuming that the cluster virialises at the redshift at which we view it. Its dependence on Ω (and therefore on redshift) is given in the lower panel of Fig 1. The assumption that clusters form at the redshift at which we view them is a good approximation in the $\Omega_0 = 1$ model since in this case halos are continuously accreting material. The value $\Delta_c = 178$, appropriate to $\Omega = 1$, has recently been shown to separate well the interior of the virialised halo from the surrounding infalling material (Cole & Lacey 1995). In low- Ω models the accretion rate onto a halo declines after $z \approx 1/(\Omega_0^{-1} - 1)$ and so little evolution in the density and temperature of the bulk of the gas takes place at low redshift. The density in the simple spherical collapse model, $\rho_{\text{crit}}^0 (1+z)^3 (\Omega_0/\Omega(z)) \Delta_c$ (where ρ_{crit}^0 is the critical density at the present day), does not accurately reproduce this behaviour but the high resolution simulations needed to determine it have yet to be carried out. Nevertheless, for the range of redshifts and Ω_0 s that we consider, the simple model is a good approximation.

The Sunyaev-Zel'dovich (Sunyaev & Zel'dovich 1972) effect is produced by the inverse Compton scattering of cosmic microwave background (CMB) photons off high energy electrons in the intracluster gas. This process distorts the blackbody spectrum by shifting microwave photons to higher energies. At long wavelengths (longward of $\lambda = 1.37$ mm for $T_{\text{CMB}} = 2.726\text{K}$), the cluster produces a negative fluctuation in the surface brightness of the CMB, while at shorter wavelengths it produces a positive fluctuation. In the long wavelength regime the microwave background decrement from the cluster is given by

$$\frac{\Delta T}{T} = -2y, \quad (2.3)$$

where y is the integral of the electron pressure along a line-of-sight through the cluster,

$$y = \int n_e \sigma_T \left(\frac{kT}{m_e c^2} \right) dl. \quad (2.4)$$

Here n_e is the number density of electrons, m_e the electron mass, and σ_T the Thompson cross-section. We can define an effective angular cross-section, Y , by integrating y over the projected area of the cluster and dividing by the square of the angular diameter distance, r_d ,

$$Y = r_d^{-2} \int y dA. \quad (2.5)$$

This quantity has a simple physical interpretation. In the long wavelength regime $2Y$ is simply the effective angular area of the microwave background obscured by the cluster. An unresolved observation of a cluster with a radio telescope of effective beam area, A_{beam} , would, in the long wavelength regime, measure a signal $\Delta T/T = -2Y/A_{\text{beam}}$. If the cluster is resolved, then the signal depends on the density profile of the cluster. Assuming a surface density proportional to R^{-1} , as in an isothermal sphere, then $\Delta T/T = -2Y/(A_{\text{clus}} A_{\text{beam}})^{1/2}$, where A_{clus} is the angular cross-section of the virialised cluster. Using the virial radius to define the edge of the cluster, we can then write

$$A_{\text{clus}} = 64.1 \beta (5X + 3) \left(\frac{kT_{\text{gas}}}{\text{keV}} \right) (1+z)^{-3} \left(\frac{\Omega(z)}{\Omega_0} \right) \times \left(\frac{\Delta_c}{178} \right)^{-1} \left(\frac{r_d}{100 \text{h}^{-1} \text{Mpc}} \right)^{-2} \text{arcmin}^2. \quad (2.6)$$

The effective angular area, Y , is also easily related to the CMB flux absorbed (or re-emitted) by the cluster at other frequencies. Defining a dimensionless frequency $x = h_p \nu / kT_{\text{CMB}} = \lambda_0 / \lambda$, where h_p is Planck's constant and $\lambda_0 = 5.28 \text{mm}$ for $T_{\text{CMB}} = 2.726 \text{K}$ (Mather *et al.* 1994), the emitted flux is

$$S_\nu(x) = S_\nu^{\text{CMB}}(x) Q(x) Y \quad (2.7)$$

$$= 2.29 \times 10^4 \frac{x^3}{e^x - 1} Q(x) \left(\frac{Y}{\text{arcmin}^2} \right) \text{mJy}, \quad (2.8)$$

where

$$Q(x) = \frac{x e^x}{e^x - 1} \left[\frac{x}{\tanh(x/2)} - 4 \right]. \quad (2.9)$$

and $1 \text{mJy} \equiv 10^{-29} \text{Js}^{-1} \text{m}^{-2} \text{Hz}^{-1}$. In the long wavelength limit, $x \rightarrow 0$, $Q(x) \rightarrow -2$ and this reduces to the result stated earlier, $\Delta T/T = S_\nu/S_\nu^{\text{CMB}} = -2Y$. At $x \approx 3.83$ ($\lambda = 1.37 \text{mm}$) $Q(x) = 0$ and at higher frequencies the cluster appears as a source of emission.

The effective cross-section, Y , defined by equations (2.4) and (2.5), is proportional to the total mass and average temperature of the intracluster gas. Specifically, for an isothermal intracluster gas,

$$Y = \frac{\sigma_T}{2m_e m_p c^2} f_{\text{ICM}} (1+X) M kT_{\text{gas}} r_d^{-2} = 9.68 \times 10^{-2} \text{h} f_{\text{ICM}} (1+X) \left(\frac{M}{10^{15} \text{h}^{-1} \text{M}_\odot} \right) \times \left(\frac{kT_{\text{gas}}}{\text{keV}} \right) \left(\frac{r_d}{100 \text{h}^{-1} \text{Mpc}} \right)^{-2} \text{arcmin}^2, \quad (2.10)$$

where f_{ICM} is the fraction of the cluster mass represented by the hot intracluster gas. We adopt $\beta = 1$ and $f_{\text{ICM}} = 0.1$ but our results can readily be rescaled to other choices. Note that here it is appropriate to use the mass-weighted temperature for which Navarro *et al.* (1995) find $\beta = 1.2$ for their $\Omega_0 = 1$ simulations.

3 COMPARISON WITH N-BODY SIMULATIONS

In order to assess the accuracy of the Press-Schechter mass distribution in the regime of interest – the mass scale of rich galaxy clusters – we compare the model predictions with the abundance of dark matter clumps found in a new set of large cosmological N-body simulations (Cole, Frenk & Weinberg in preparation). The simulations were performed with the AP³M code of Couchman (1991) using $192^3 \approx 7 \times 10^6$ particles in a periodic box of size $l_{\text{box}} = 345.6 \text{h}^{-1} \text{Mpc}$. The particle mass was $M_p = 1.64 \times 10^{12} \Omega_0 \text{h}^{-1} \text{M}_\odot$ and the force resolution $\epsilon = 180 \text{h}^{-1} \text{kpc}$, where ϵ is the equivalent Plummer potential softening parameter. Two sequences of simulations were carried out with different values of Ω_0 , a sequence of open models with $\Lambda_0 = 0$ and a sequence of flat models with $\Omega_0 + \Lambda_0 = 1$. Both were normalised to have $\sigma_8 = 0.55 \Omega_0^{-0.6}$ so as to reproduce, approximately, the observed abundance of galaxy clusters (White *et al.* 1993). The number of timesteps required to evolve the simulations accurately from the linear regime to the present epoch was approximately $100/\Omega_0$. The initial linear power spectrum was the same in all simulations, a CDM-like spectrum with scale parameter $\Gamma = \Omega_0 \text{h} = 0.25$. This value of Γ is suggested by observations of large-scale galaxy clustering (eg. Maddox *et al.* 1990). Here we will consider only three representative models, one with $\Omega_0 = 1$, another with $\Omega_0 = 0.3$ and $\Lambda_0 = 0$, and a third one with $\Omega_0 = 0.3$ and $\Lambda_0 = 0.7$.

We identified groups of particles in the simulations using two different algorithms. The first was the standard friends-of-friends algorithm (Davis *et al.* 1985) with linking length b_l times the mean interparticle separation; the second was the spherical overdensity algorithm (Lacey & Cole 1994) with density contrast κ_ρ . We chose values of b_l and κ_ρ so that, on average, groups have the overdensity characteristic of virialised objects predicted by the spherical collapse model. For the friends-of-friends linking length we took $b_l = 0.2$ in the $\Omega_0 = 1$ simulation and scaled as $b_l \propto (\Delta_c/\Omega)^{-1/3}$ for the other cases. In both the simulations and the Press-Schechter model we converted mass to temperature using relation (2.2).

Fig 2 compares cluster abundances as a function of kT at $z = 0$ and $z = 0.5$ in the N-body simulations and in the Press-Schechter model. Overall, the analytical predictions are in excellent agreement with the N-body results and reproduce the near exponential fall-off of the temperature functions very accurately. The threshold density, δ_c , has *not* been treated as a free parameter, but has instead been fixed at the value prescribed by the spherical collapse model. For the $\Omega_0 = 1$ case at $z = 0$ this value is essentially perfect and produces a temperature function midway between that obtained using the friends-of-friends and spherical overdensity algorithms. For $z = 0.5$, the spherical overdensity algorithm finds somewhat fewer high tempera-

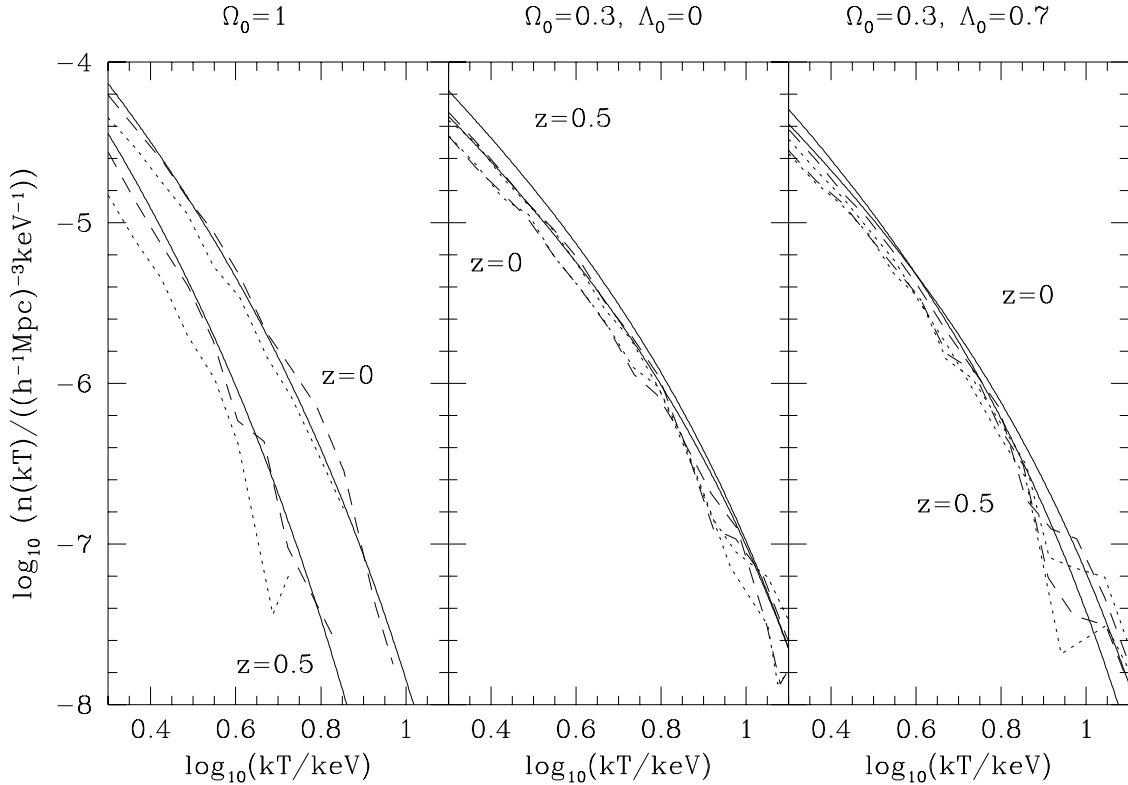


Figure 2. Comparison of the temperature functions predicted by the Press-Schechter distribution and the results of N-body simulations. For each of the three cosmological models (with parameters given at the top of each panel), temperature functions are plotted for $z = 0$ and $z = 0.5$. The Press-Schechter predictions, which are normalised according to the spherical collapse model, are shown by solid lines. The simulation results are plotted with dashed lines for clusters identified with a friends-of-friends algorithm and with dotted lines for clusters found with the spherical overdensity algorithm. Over the full range of abundances and redshifts shown the agreement between theory and simulations is very good.

ture clusters than either the friends-of-friends algorithm or the Press-Schechter model. This may partially reflect the relatively low resolution of the N-body simulations as the most massive groups contain only about 100 particles in the $\Omega_0 = 1$ simulation at $z = 0.5$. In the two $\Omega_0 = 0.3$ cases, the Press-Schechter model matches the very slow evolution of the halo abundances in the simulations extremely well. If one were to adjust δ_c upwards by approximately 4%, then the N-body results would be reproduced almost perfectly over the temperature range plotted in Fig 2. However, such a small adjustment is negligible compared to the uncertainty in the abundance of real clusters. We note that for the more common, lower temperature clusters not shown in this figure, the Press-Schechter distribution predicts a significantly higher abundance than found in the simulations. We conclude that, for the range of masses of interest, the agreement with the numerical results is sufficiently good that we can confidently use the Press-Schechter model for detailed calculations.

4 NORMALISATION OF THE MODELS

We now compare the predicted and observed distributions of cluster X-ray temperatures in the local universe in order to obtain an estimate of σ_8 , the *rms* mass fluctuation in spheres of radius $8h^{-1}\text{Mpc}$. The observational data we use is the complete flux-limited sample of 25 clusters com-

puted by Henry & Arnaud (1991). We compare our estimate with earlier determinations of σ_8 from both X-ray and optical data (Henry & Arnaud 1991; White *et al.* 1993; Viana & Liddle 1995) and discuss the reasons why these earlier determinations gave slightly different values of σ_8 .

The stepped curve in Fig 3 shows the following simple estimate of the cumulative cluster temperature function derived from the Henry & Arnaud data,

$$N(> kT) = \sum_{kT_i > kT} 1/V_{\text{max},i}, \quad (4.1)$$

where $V_{\text{max},i}$ is the maximum volume in which the cluster could be detected given the flux limit and geometric boundaries of the survey. We have chosen to present the results in cumulative form in order to avoid binning the data. Since the cluster abundance falls very rapidly with increasing temperature, the differential temperature function averaged over each bin can be significantly larger than the underlying unbinned distribution. Henry & Arnaud (1991) estimated the differential temperature function by weighting the number of clusters in each temperature bin with the *average* value of $V_{\text{max},i}$ in that bin. This estimator is only equivalent to (4.1) if $V_{\text{max},i}$ is the same for all of the clusters in each bin. However, since the bins have non-zero width and the L_X-T_X relation has considerable scatter, there is also considerable scatter in the individual $V_{\text{max},i}$ values in each temperature bin. For the Henry & Arnaud dataset this is a large effect and would have led them to underestimate the cluster abundance by

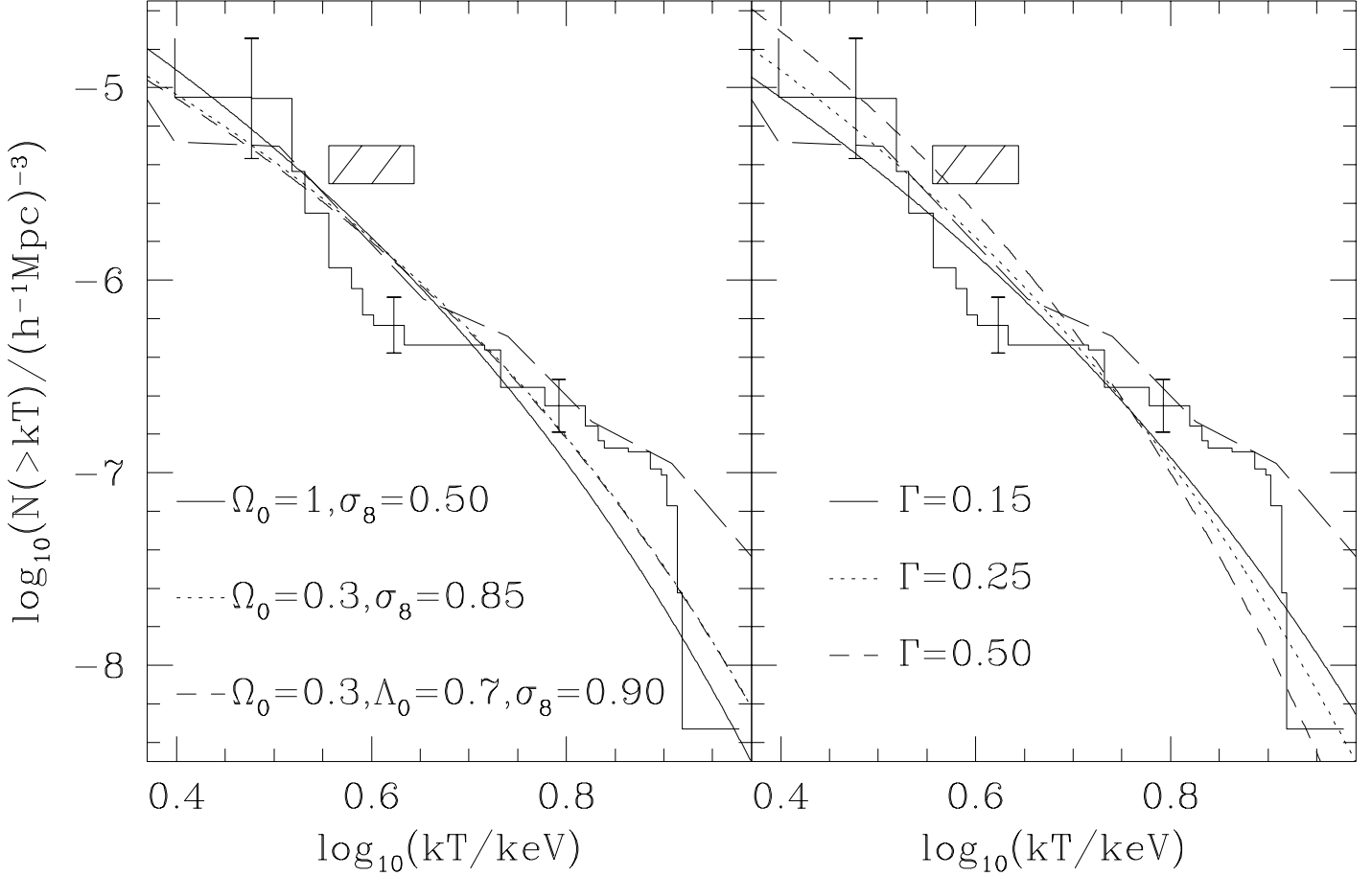


Figure 3. Predicted and observed X-ray temperature functions. The left-hand panel shows model predictions for $\Gamma = 0.25$ and $\Omega_0 = 1$ (smooth solid line), $\Omega_0 = 0.3$, $\Lambda_0 = 0$ (dotted line) and $\Omega_0 = 0.3$, $\Lambda_0 = 0.7$ (dashed line). The models are normalised by fitting to the observed data as described in the text. The observed temperature function, shown as a solid line with steps, was derived from the data compiled by Henry & Arnaud (1991). The error bars at the three temperatures where the models were fit were obtained from a bootstrap analysis. The best-fit values of σ_8 are given in the figure. The long-dashed line shows the cumulative temperature function obtained by Edge *et al* (1990). The hatched box represents the range of normalisations derived by White, Efstathiou & Frenk (1993) from a similar theoretical analysis of combined X-ray and optical data. The right-hand panel gives model predictions for $\Omega = 1$, $\sigma_8 = 0.5$ and three values of Γ : 0.15 (solid line), 0.25 (dotted line), and 0.50 (dashed line). The observational data and the hatched box are the same as in the left-hand panel.

approximately a factor of 4. However, (Henry private communication) in computing each $V_{\max,i}$, a spurious factor of 4.2 entered their calculation and this largely compensated for the bias in the estimator. Thus the published Henry & Arnaud (1991) temperature function is in reasonably good agreement with our estimate. It is also in reasonable agreement with the cumulative temperature function of Edge *et al.* (1990), reproduced as the long dashed line in Fig 3.

To estimate σ_8 , we fit our model predictions to our estimate of the temperature function. First, we calculate the statistical errors in the temperature function through a bootstrap procedure. At three selected temperatures, T_i , we computed (using equation 4.1) the temperature function for a large number of samples of 25 clusters constructed by randomly selecting, with replacement, from the original list of 25 clusters in Henry & Arnaud's compilation. The error bars in Fig. 3 show the resulting $1 - \sigma$ ranges in the bootstrap distribution of $\log_{10} N_{\text{boot}}(> kT)$, at our three chosen temperatures. This distribution was also used to compute the

covariance between the estimates at different temperatures. Averaging over the bootstrap samples we thus obtain the covariance matrix,

$$C_{ij} = \langle \epsilon_i \epsilon_j \rangle, \quad (4.2)$$

where $\epsilon_i = \log_{10} N_{\text{boot}}(> kT_i) - \log_{10} N_{\text{data}}(> kT_i)$. We then fit the model temperature functions by minimising

$$\chi^2 = \sum_{ij} \delta_i C_{ij}^{-1} \delta_j, \quad (4.3)$$

where $\delta_i = \log_{10} N_{\text{model}}(> kT_i) - \log_{10} N_{\text{data}}(> kT_i)$. If the data points are uncorrelated C_{ij} is diagonal and equation (4.3) reduces to the normal definition of χ^2 . We find that there are significant correlations between the estimates of $\log_{10} N(> kT)$ at the three selected temperatures, but that the models which minimise χ^2 are insensitive to whether the correlations are treated as above or simply ignored.

The best-fit models are shown in Fig 3 for $\Omega_0 = 1$ and

$\Omega_0 = 0.3$, with and without a cosmological constant. The models in the left-hand panel all have the same CDM-like power spectrum with $\Gamma = 0.25$. Because of the very sensitive dependence of cluster abundance on spectrum normalisation, σ_8 can be estimated with high precision even though the errors in the empirical cluster abundance are quite large. The formal error on σ_8 from the fits in Fig 3 is $\pm 2\%$, but this is likely to be an underestimate of the true uncertainty because, with only 25 clusters, the errors in the temperature function are unlikely to be Gaussian and, in addition, systematic errors are likely to be significant.

The right-hand panel of Fig 3 shows the effect of allowing Γ to vary for the case of $\Omega_0 = 1$. Values of $\Gamma < 0.25$ produce more large scale power and more very hot clusters. This produces a temperature function with a shallower slope, which is in better agreement with the observations. (The best fitting model has $\Gamma = 0.03$ and $\sigma_8 = 0.51$, but this is not a reliable way of constraining Γ because the high and low temperature points are anticorrelated, and this creates a large uncertainty in the slope of the temperature function.) Fortunately, the best fitting values of σ_8 are quite insensitive to the adopted value of Γ , because as Γ varies it is the slope of the temperature function that varies with the pivot point remaining in the middle of the range of rich cluster temperatures. This simply reflects the fact noted above that the average mass within a sphere of radius $8h^{-1}\text{Mpc}$ in an unperturbed universe with $\Omega_0 \approx 1$ is very close to the mass of a rich galaxy cluster.

In summary, we find that the observed temperature function is well fit by all our CDM-like models if

$$\sigma_8 = (0.50 \pm 0.01)\Omega_0^{-0.47+0.10\Omega_0} \quad \text{for } \Lambda_0 = 0 \quad (4.4)$$

and

$$\sigma_8 = (0.50 \pm 0.01)\Omega_0^{-0.53+0.13\Omega_0} \quad \text{for } \Omega_0 + \Lambda_0 = 1. \quad (4.5)$$

The quoted statistical uncertainty corresponds to the standard deviation of the σ_8 values obtained from fitting the individual bootstrap catalogues. A more realistic estimate of the error would take into account the variation of σ_8 due to the uncertainty in the measured X-ray temperatures and the values of both δ_c and β . The error in δ_c we estimate from Fig. 2 to be $\lesssim 4\%$. The uncertainty in the appropriate β we take to be 10% (see Navarro *et al.* 1995). Note that adopting $\beta = 1.1$ leads to values of σ_8 which are 6% larger than those quoted above. Combining these sources of error we estimate the overall uncertainty in σ_8 to be approximately 8%, which is four times as large as the statistical error shown in equations (4.4) and (4.5).

The values of σ_8 that we infer from the X-ray data are systematically lower than those obtained by White *et al.* (1993) who found $\sigma_8 = 0.57\Omega_0^{-0.56}$. Our modelling of the cluster abundances is almost identical and the difference in our inferred values of σ_8 results almost entirely from the different observational data that we fitted. White *et al.* estimated the mass of clusters with abundance $4 \times 10^{-6}h^3\text{Mpc}^{-3}$ in two different ways. The first and larger estimate was based on the median velocity dispersion of rich Abell clusters. The second was based on the cumulative temperature functions of Henry & Arnaud (1991) and Edge *et al.* (1990). The range spanned by these two estimates, expressed as a temperature rather than a mass using equation (2.2), is indicated by the hatched box in Fig 3. The lower estimate of the X-ray tem-

perature is slightly higher than our analysis of the Henry & Arnaud data implies. This difference is due to the fact that the White *et al.* estimate was inferred indirectly from the differential temperature function presented by Henry & Arnaud, not directly from the cumulative temperature function. (If we adopt $\sigma_8 = 0.57\Omega_0^{-0.56}$ then our model temperature curves pass through the shaded box in agreement with White *et al.*).

Henry & Arnaud (1991) found $\sigma_8 = 0.59 \pm 0.02$ for $\Omega_0 = 1$ and a power-law fluctuation spectrum. They used essentially the same data as us, but they adopted $\beta = 1.2$ in equation (2.2), while we have assumed $\beta = 1$. Thus, for the same value of σ_8 , their model temperature functions are shifted to lower temperatures by ~ 0.08 in $\log_{10}(kT)$, and this largely accounts for the difference in the inferred values of σ_8 . Viana & Liddle (1995) obtained $\sigma_8 = 0.6$ for $\Omega_0 = 1$, with a dependence on Ω_0 close to that which we find, by fitting only to the abundance of clusters at 7keV. It may be seen from Fig 3 that fitting the cumulative temperature function just at this temperature yields a higher value of σ_8 than the one obtained from fitting all the X-ray data. Given the small number of clusters with temperatures as great as 7keV, fitting over a wider temperature range seems more appropriate.

In summary, our modelling of the cluster temperature function is consistent with those of Henry & Arnaud (1991), White *et al.* (1993) and Viana & Liddle (1995). The range in the values of σ_8 deduced by these authors arises from the different data points they chose to fit and, in the case of Henry & Arnaud (1991), from the value of β they used to relate virial to gas temperature. Assuming $\beta = 1$, we conclude that the X-ray data are best fit by the values of σ_8 given by equations (4.4) and (4.5). Since the abundance of Abell clusters of richness class ≥ 1 is $8 \times 10^{-6}h^3\text{Mpc}^{-3}$, our results imply that the median 1-D virial velocity dispersion of these clusters should be approximately 650km s^{-1} . This is smaller than the median values of around 800km s^{-1} , found in the compilations of Zabludoff, Huchra & Geller (1990) and Girardi *et al.* (1993). These differences may be understood if, as argued by Frenk *et al.* (1990) and others, the higher velocity dispersion estimates are artificially boosted by contamination from infalling groups around the cluster. Alternatively, these larger velocity dispersions (and a higher value of σ_8) would be consistent with the X-ray data if the intracluster gas were significantly cooler than the virial temperature, but this would require $\beta \gtrsim 1.5$. Such large values of β are not supported either by the data or by recent hydrodynamic simulations of cluster formation (Navarro *et al.* 1995, Evrard *et al.* 1995).

5 CLUSTER EVOLUTION

Having fixed the normalisation of the models by requiring that they should match the local abundance of rich clusters, we now consider their evolutionary properties. Specifically, we calculate the redshift dependence of the mass function, X-ray temperature function and the distribution of S-Z decrements. For each model, the evolution of the cluster mass function (equation (2.1) is governed by the linear growth factor, $D(z, \Omega_0, \Lambda_0)$. The evolution of the X-ray temperature and S-Z effect depends, in addition, on the evolu-

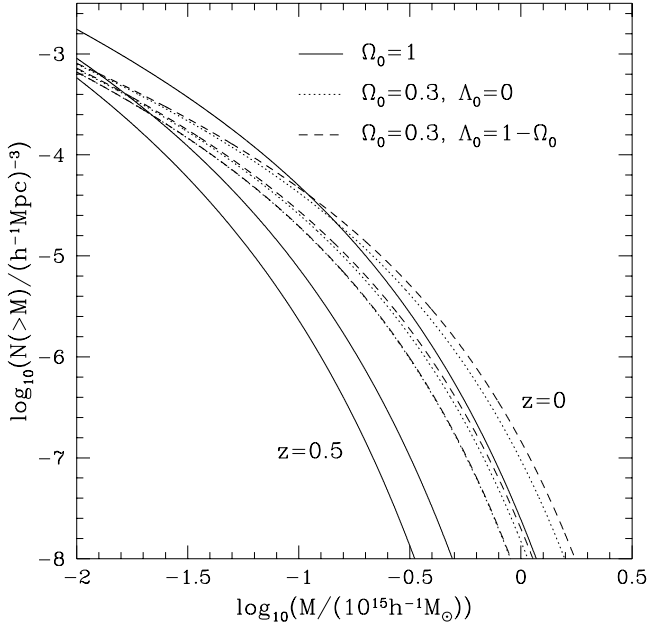


Figure 4. Predicted evolution of the cluster mass function. The comoving number density of clusters per $(h^{-1}\text{Mpc})^3$ with masses larger than M is shown as a function of M . Solid lines correspond to $\Omega = 1$; dotted lines to an open model with $\Omega_0 = 0.3$; and the dashed lines to a flat model with $\Omega_0 = 0.3$ and $\Lambda_0 = 0.7$. Predictions for $z = 0$, $z = 0.33$ and $z = 0.5$ are plotted. There is relatively little evolution in the $\Omega_0 < 1$ cosmologies but, in an $\Omega_0 = 1$ model, the abundance of clusters declines precipitously with redshift.

tion of the virial density $\Delta_c \Omega_0 / \Omega(z)$, which determines the relation (2.2) between mass and temperature.

5.1 Evolution of the cluster mass function

The growth of fluctuations continues at a rapid rate at recent times if $\Omega_0 = 1$ and very little if $\Omega_0 = 0.3$. As a result, the rich cluster mass function evolves dramatically between $z = 0.5$ and $z = 0$ if $\Omega_0 = 1$, but much less so if Ω_0 is low, whether or not the cosmological constant is zero. This evolution is illustrated in Fig 4. For $\Omega_0 = 1$, the comoving number density of clusters of virial mass $M = 3.5 \times 10^{14} h^{-1} M_\odot$, typical of Abell clusters of richness class $R \geq 1$, declines by a factor of 30 between $z = 0$ and $z = 0.33$ and, by $z = 0.5$, it is tiny. By contrast, for $\Omega_0 = 0.3$, $\Lambda_0 = 0.7$, the abundance of clusters of this mass has only dropped by a factor of ~ 7 below the present day abundance even at $z = 0.5$; if $\Lambda_0 = 0$ the decline is even slower.

The strong Ω_0 -dependence of the rate at which the mass function evolves is reflected in the expected redshift distributions of massive clusters ($M > 3.5 \times 10^{14} h^{-1} M_\odot$), illustrated in the top panel of Fig 5. For $\Omega_0 = 1$ the distribution peaks sharply at very low redshift, whereas for low Ω_0 a broader peak is displaced to higher redshift. The effect of Λ_0 is to move the peak back to a somewhat lower redshift, reflecting the slightly later epoch at which structure ceases to grow in non-zero Λ_0 cosmologies.

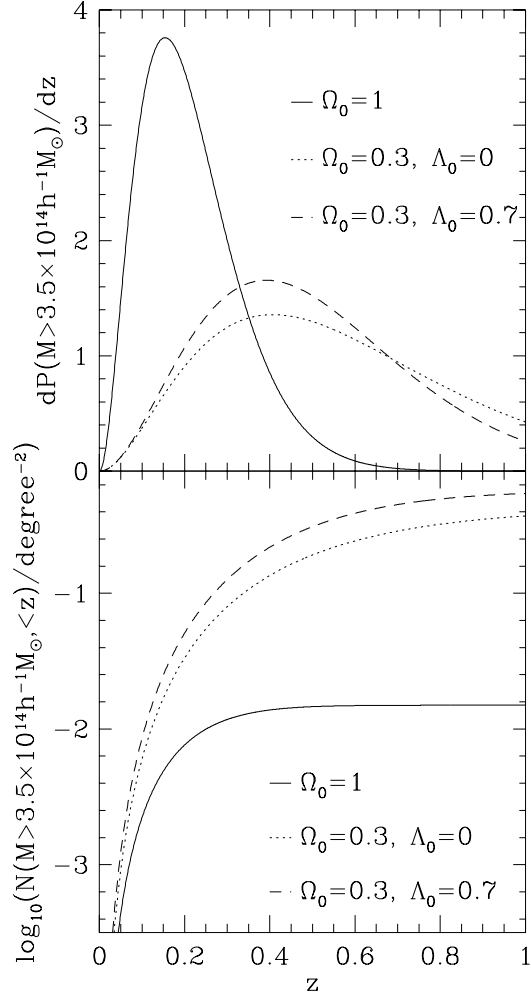


Figure 5. *Upper panel:* Redshift distribution of massive clusters ($M > 3.5 \times 10^{14} h^{-1} M_\odot$) in different cosmological models. The ordinate gives the probability distribution of clusters per unit redshift interval. *Lower panel:* Number counts of clusters with mass $M > 3.5 \times 10^{14} h^{-1} M_\odot$ out to a given redshift. The ordinate gives the count per unit area on the sky. In both panels solid lines correspond to $\Omega_0 = 1$, dotted lines to $\Omega_0 = 0.3$ and dashed lines to $\Omega_0 = 0.3, \Lambda_0 = 0.7$. The models are normalised by the value of σ_8 for which the predicted temperature function at $z = 0$ best fits the data. The low- Ω_0 cosmologies produce significantly more clusters at high redshifts than the $\Omega_0 = 1$ model.

Integrating over the redshift distributions yields the number count of clusters per unit area on the sky. The change in the volume element corresponding to a fixed redshift interval enhances the differences between the high and low- Ω models. At redshift $z = 0.33$, the volumes per unit redshift are in the ratios 1 : 1.23 : 1.7 for $\Omega_0 = 1$, $\Omega_0 = 0.3$, $\Lambda_0 = 0$ and $\Omega_0 = 0.3$, $\Lambda_0 = 0.7$ respectively. At $z = 0.5$ the corresponding ratios increase to 1 : 1.35 : 2.02. Thus, for $\Omega_0 = 1$, we expect to find only 0.015 clusters per square degree with mass greater than $3.5 \times 10^{14} h^{-1} M_\odot$ out to $z = 0.5$ and virtually none at higher redshifts. By contrast, for $\Omega_0 = 0.3$, we expect to find more than 10 times as many

clusters above this mass with $z < 0.5$. Note that predictions for low- Ω models are relatively insensitive to the value of Λ_0 , with only about 50% more clusters predicted to exist in the non-zero Λ_0 model. This factor results largely from the difference in the volume elements.

The cluster mass that enters into equation (2.1) and Figs 4 and 5 is the virial mass, *ie* the mass contained within a sphere of mean overdensity Δ_c . In practice, gravitational lensing measurements give the mean projected surface density, $\Sigma(R)$, within a radius, R , which is typically less than $1h^{-1}\text{Mpc}$. To relate these two masses requires a model of the cluster mass distribution. Recent high resolution N-body simulations show that, over most of the cluster, the dark matter density profile is well approximated by an isothermal profile (Navarro *et al.* 1995; Cole & Lacey 1996). Although in principle it would be straightforward to use the analytical fit to the N-body profile given by Navarro *et al.* (1995), for our purposes the isothermal profile approximation is quite adequate. In this case, mean surface density is related to virial mass by

$$M_{\text{vir}} = \frac{4}{H} \left(\frac{GR^3\Sigma(R)^3}{\Delta_c} \right)^{1/2}, \quad (5.1)$$

where R is any radius inside the virial radius, H is Hubble's constant at the redshift of the cluster and the overdensity Δ_c is given in Fig 1 as a function of Ω . This formula may be used to relate the surface mass density estimated from weak gravitational lensing analyses to the virial mass used throughout this paper. Note, however, that we have implicitly assumed that any foreground or background mass makes a negligible contribution to the lensing signal.

5.2 Evolution of the X-ray temperature function

The evolution of the X-ray temperature function depends both on the growth factor, $D(z, \Omega_0, \Lambda_0)$, and on the virial density, $\Delta_c \Omega_0 / \Omega(z)$. Thus, at high z , the abundance of clusters of a given temperature is determined by the balance between the overall decline in the population of virialized clusters and the lower mass associated with each temperature. If $\Omega_0 = 1$, the first factor is dominant and the temperature function declines precipitously (see Fig 6). By contrast, in an open, $\Omega_0 = 0.3$, universe, the two effects nearly cancel out and the temperature function remains virtually unchanged at least out to $z = 0.5$. A flat, $\Omega_0 = 0.3$, universe is intermediate and, in this case, the temperature function declines slowly with redshift.

The redshift distribution of clusters hotter than 5 keV is shown in Fig 7. As was the case for the mass function, the $\Omega_0 = 1$ model produces large clusters predominantly at low redshifts. The $\Omega_0 = 0.3$ models, on the other hand, give rise to extended redshift distributions. Again, the lower redshift at which structure ‘‘freezes-out’’ when a Λ_0 term is included produces somewhat stronger evolution in this case compared to an open cosmology. When integrating over redshift, the effect of different evolutionary rates is enhanced by the larger volume in low density universes. As a result, the number counts per unit area of sky, displayed in the lower panel of Fig 7, depend strongly on the value of Ω_0 . For our choice of parameters, the counts in the two $\Omega_0 = 0.3$ models are very similar and the total number of clusters hotter than

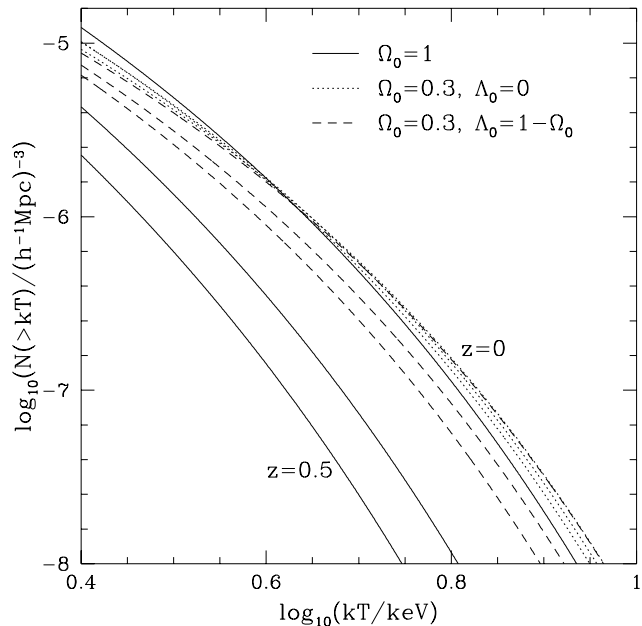


Figure 6. Predicted evolution of the cluster X-ray temperature function. The comoving number density of clusters per $(h^{-1}\text{Mpc})^3$ hotter than kT is shown as a function of kT . Solid lines correspond to $\Omega = 1$; dotted lines to an open model with $\Omega_0 = 0.3$; and the dashed lines to a flat model with $\Omega_0 = 0.3$ and $\Lambda_0 = 0.7$. Predictions for $z = 0$, $z = 0.33$ and $z = 0.5$ are plotted. There is little evolution in the $\Omega_0 < 1$ cosmologies but in an $\Omega_0 = 1$ model, the abundance of clusters declines precipitously with redshift.

5 keV at redshifts less than 0.5 is about 9 times higher in these models than in the $\Omega_0 = 1$ case. The expected number counts for different values of Ω_0 are shown in Fig 8, for both open and flat models.

We emphasize that the results shown in Figs 6 - 8 are very sensitive to the normalisation of the fluctuation amplitude. Our adopted values of σ_8 were fixed by requiring that each model should agree well with the present day X-ray temperature function. With this particular choice, the inclusion of a Λ_0 term turns out to make very little difference to the predicted abundance of hot clusters out to redshift of 0.5. However, the number counts out to this redshift do discriminate well between different values of Ω_0 .

5.3 Evolution of Sunyaev-Zel’dovich effect

As discussed in Section 2, we characterize the S-Z effect by the Y -function given in equations (2.5) and (2.10). (Here, we take $f_{\text{ICM}} = 0.1$ and $\beta = 1$, but our results are readily scaled to other values using $Y \propto f_{\text{ICM}}\beta^{-1}$.) The evolution of the Y -function is similar to that of the temperature function, but since $Y \propto M^{5/3}$ whilst $T \propto M^{2/3}$, the detailed behaviour is slightly different. More importantly, the appearance of the diameter-distance in equation (2.5) causes Y to drop off with redshift more rapidly than kT .

Figure 9 confirms the rapid decline in the Y -function with redshift, resulting from the r_d^{-2} term, in all our cosmo-

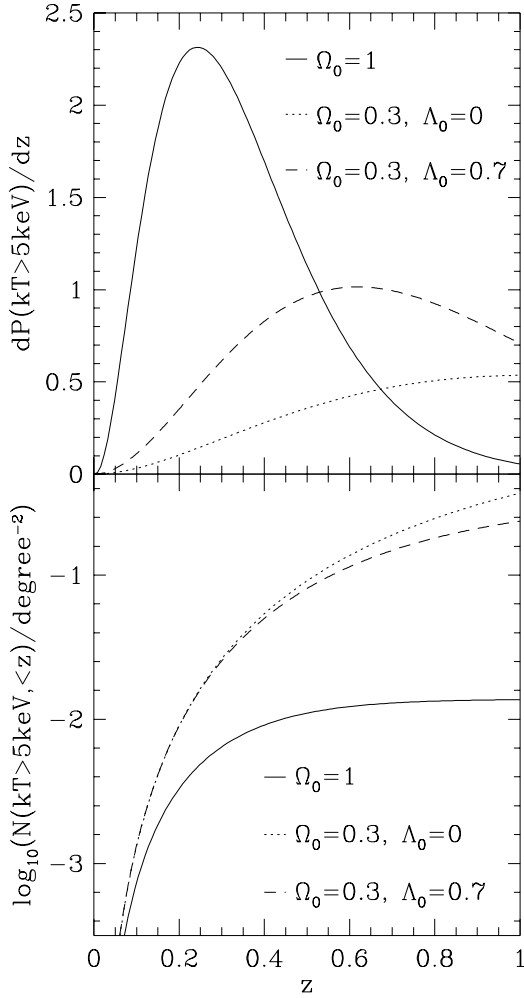


Figure 7. *Upper panel:* Redshift distribution of hot clusters ($kT > 5\text{keV}$) in different cosmological models. The ordinate gives the probability distribution of clusters per unit redshift interval. *Lower panel:* Number counts of clusters hotter with $kT > 5\text{keV}$ out to a given redshift. The ordinate gives the count per unit area on the sky. In both panels solid lines correspond to $\Omega_0 = 1$, dotted lines to $\Omega_0 = 0.3$ and dashed lines to $\Omega_0 = 0.3, \Lambda_0 = 0.7$. The models are normalised by the value of σ_8 for which the predicted temperature function at $z = 0$ best fits the data. The low- Ω_0 cosmologies produce significantly more clusters at high redshifts than the $\Omega_0 = 1$ model.

logical models (which, as before, are normalised using the local cluster X-ray temperature function). Evolution is in the same sense as evolution in the cluster mass and X-ray temperature functions. Also, for $z > 0$, the differences between the Y -functions of our various models are of similar magnitudes. To understand why this is so we need to consider the two factors mentioned above. In the $\Omega_0 = 1$ model, in which the fluctuation growth factor is still changing rapidly at low redshifts, $M^{5/3}$ decreases faster with redshift than either M , which is relevant to the mass function, or $M^{2/3}$, which is relevant to the temperature function. Thus, for $\Omega_0 = 1$, the Y -function evolves more rapidly than the mass or temper-

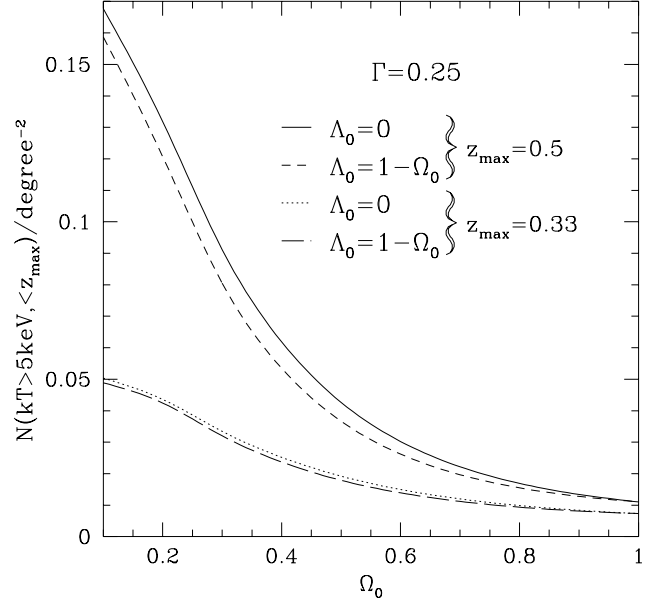


Figure 8. Predicted number counts of clusters hotter than 5 keV out to $z = 0.33$ and 0.5, as a function of Ω_0 . The solid and dotted lines correspond to open models ($\Lambda_0 = 0$) and the dashed lines to flat models ($\Lambda_0 = 1 - \Omega_0$). The abundances are sensitive to the choice of σ_8 , but the ratio of the numbers expected in different cosmologies is less so.

ature functions. This is partly offset, in the low- Ω_0 models, by their larger angular-diameter distance out to a particular redshift.

Because of the strong evolution apparent in Fig 9, the redshift distribution of “S-Z bright” clusters is highly peaked at low redshift in all our models. This distribution is plotted in Fig 10 for clusters with $Y > 10^{-3} \text{ h arcmin}^2$. The corresponding number counts as a function of Ω_0 are shown in Fig 11. The counts are dominated by local clusters and, since all the models are normalised to the local temperature function, the counts are similar in all cases. Nevertheless, $\sim 60\%$ more $Y > 10^{-3} \text{ h arcmin}^2$ clusters are expected if $\Omega_0 = 0.3$ than if $\Omega_0 = 1$. The splitting between the various cosmologies increases if the Y threshold is reduced, as illustrated in Fig 12. As the threshold is lowered, the counts probe higher redshifts where the predictions are increasingly sensitive to Ω_0 . Thus, if the threshold is taken to be $10^{-4} \text{ h arcmin}^2$, over twice as many clusters are expected per unit area if $\Omega_0 = 0.3$ than if $\Omega_0 = 1$. As with the counts as a function of mass or X-ray temperature, the counts as a function of Y are insensitive to Λ_0 . The redshift distribution of a sample of Y -selected clusters gives a more promising method of constraining Ω_0 . For clusters with $Y > 10^{-3} \text{ h arcmin}^2$ the median redshift (see Fig. 10) in the two $\Omega_0 = 0.3$ models is approximately $\bar{z} = 0.136$, which is a little over twice that of the $\Omega_0 = 1$ model. Thus optical follow up on a relatively small sample of Y -selected clusters could easily distinguish between these two models.

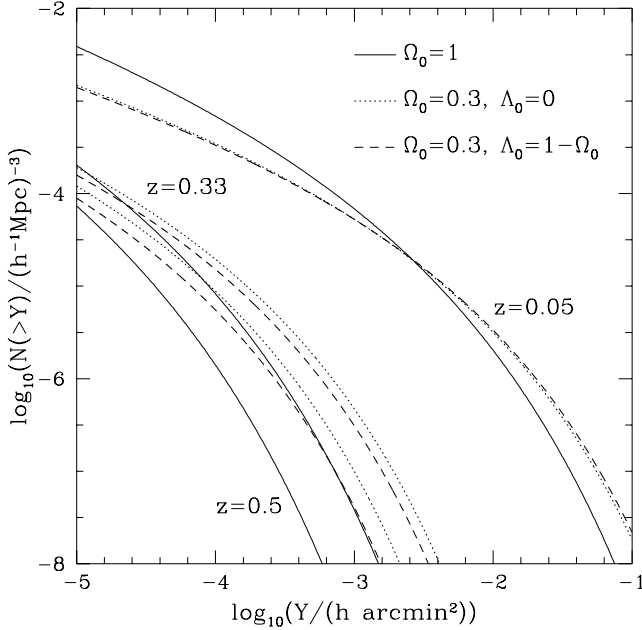


Figure 9. Predicted evolution of the cumulative cluster S-Z Y-function. The ordinate gives the comoving number density of clusters per $(h^{-1}\text{Mpc})^3$. The solid lines are for $\Omega_0 = 1$; the dotted lines for $\Omega_0 = 0.3$ and the dashed lines for $\Omega_0 = 0.3$ and $\Lambda_0 = 0.7$. Predictions for $z = 0.05$, $z = 0.33$ and $z = 0.5$ are plotted. The Y-function evolves significantly in the three cosmologies, but the evolution is strongest for $\Omega_0 = 1$.

6 DISCUSSION AND CONCLUSIONS

We have used the Press-Schechter formalism to investigate the evolution of the population of rich galaxy clusters. Our work extends and complements earlier work using this formalism by Evrard (1989), Henry & Arnaud (1991), Lilje (1992), Oukbir & Blanchard (1992), Hanami (1993), White *et al.* (1993), Barbosa *et al.* (1995), Hattori & Matsuzawa (1995), and Viana & Liddle (1995), amongst others. We first verified that the Press-Schechter formula predicts the correct abundance of rich clusters at $z = 0$ and $z = 0.5$ by comparing with the results of large cosmological N-body simulations. The agreement is excellent, at least for the models we have considered: CDM-like cosmologies with spectral shape parameter, $\Gamma = 0.25$ and with (a) $\Omega_0 = 1$, (b) $\Omega_0 = 0.3$, $\Lambda_0 = 0$ and (c) $\Omega_0 = 0.3$, $\Lambda_0 = 0.7$.

We reconsidered the problem of normalising the amplitude of mass fluctuations on cluster scales by reference to the present day abundance of rich clusters. From our own rederivation of the X-ray temperature distribution of clusters, using Henry & Arnaud's (1991) data, we found the following values for the *rms* density fluctuation in spheres of radius $8h^{-1}\text{Mpc}$, σ_8 :

$$\sigma_8 = (0.50 \pm 0.04)\Omega_0^{-0.47+0.10\Omega_0} \quad \text{for } \Lambda_0 = 0 \quad (6.1)$$

and

$$\sigma_8 = (0.50 \pm 0.04)\Omega_0^{-0.53+0.13\Omega_0} \quad \text{for } \Omega_0 + \Lambda_0 = 1. \quad (6.2)$$

For $\Omega_0 = 1$ this estimate is independent of the shape of

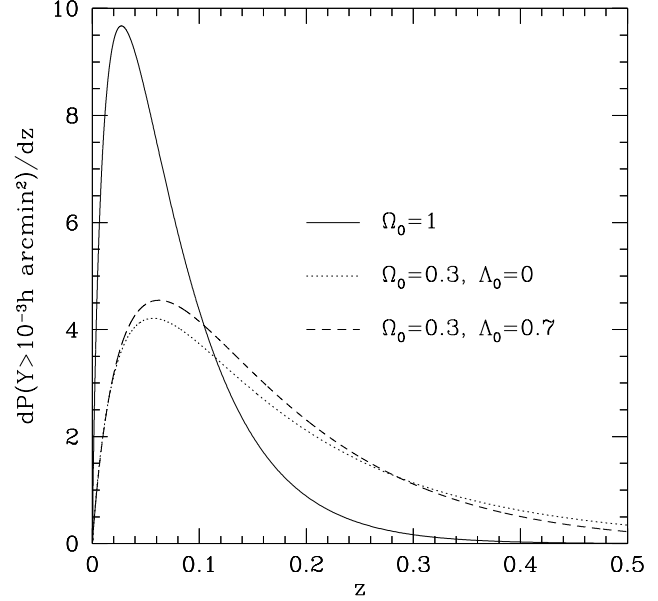


Figure 10. Redshift distribution of S-Z bright clusters ($Y > 10^{-3}h \text{ arcmin}^2$) in different cosmological models. The ordinate gives the probability distribution of clusters per unit redshift interval. The solid line corresponds to $\Omega_0 = 1$, dotted line to $\Omega_0 = 0.3$ and dashed line to $\Omega_0 = 0.3$ and $\Lambda_0 = 0.7$.

the power spectrum and, for other values of Ω_0 , there is only a very weak dependence. Note that σ_8 is only slightly larger if the Λ term is non-zero. For $\Omega_0 > 0.2$, the difference between the flat and open models is always less than 10%. Note also that since the *rms* fluctuation in the bright galaxy distribution is 0.96 (Maddox, Efsthathiou, & Sutherland 1996) in spheres of radius $8h^{-1}\text{Mpc}$, our estimates of σ_8 imply that the biasing parameter defined as $b = 0.96/\sigma_8$ is greater than unity for open models with $\Omega_0 > 0.23$ and for flat models with $\Omega_0 > 0.27$. Models with Ω_0 smaller than this require antibiasing, that is they require bright galaxies to be less clustered than the mass. Our estimates of σ_8 differ slightly from those obtained by previous authors and, in Section 4, we discussed in detail the reasons for these differences.

The quoted uncertainties in equations (6.1) and (6.2) represent the estimated overall errors in the model fits to the observed X-ray temperature function. The main source of uncertainty in our analysis is our modelling of the X-ray emitting intracluster medium as a homogeneous, isothermal gas in hydrostatic equilibrium (cf equation 2.2). There is some tentative evidence from ASCA data that the temperature in some clusters may be declining at large radii (Markevitch *et al.* 1996). On the other hand, hydrodynamic simulations show that the isothermal assumption is a good approximation in the region where most of the X-rays are emitted, at least in the case where cooling flows are ignored (Evrard 1990, Tsai, Katz & Bertschinger 1994, Navarro *et al.* 1995). Our modelling also required us to fix a value of the parameter β , the ratio of specific galaxy kinetic energy to specific gas thermal energy, and we chose to set $\beta = 1$,

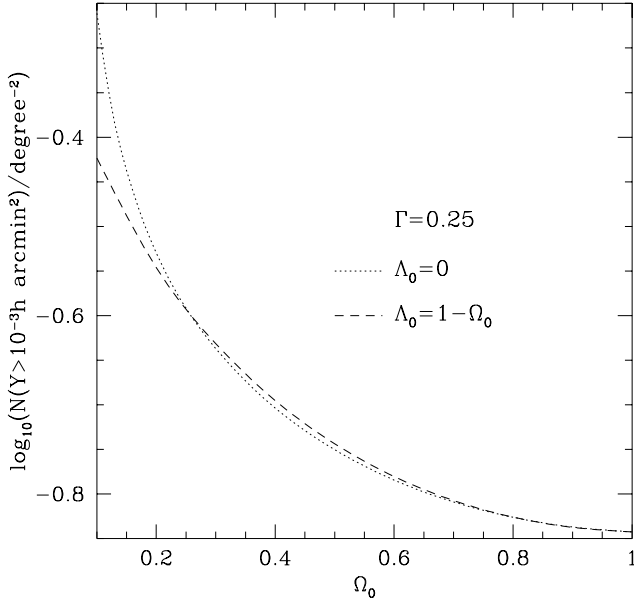


Figure 11. Predicted number counts of S-Z clusters with $Y > 10^{-3}h \text{ arcmin}^2$ out to $z = 0.33$ and 0.5 as a function of Ω_0 . The dotted line corresponds to open models ($\Lambda_0 = 0$) and the dashed line to flat models ($\Lambda_0 = 1 - \Omega_0$). The fractional difference between the models is smaller than in the corresponding plot for the temperature function because the counts are dominated by objects at low redshift where the models have been normalised to match the observed temperature function.

consistent with the results of simulations. If bulk motions or magnetic stresses contribute to the support of the gas, a larger value of β would be appropriate. In this case, our results may be recast by scaling all temperatures inversely with β and this would lead to higher estimates of σ_8 . Finally, the estimated gas temperatures and our inferred values of σ_8 may also be underestimated if small-scale inhomogeneities in the gas distribution affect the measured X-ray spectrum.

The values of σ_8 required to match the local abundance of clusters may be compared with measurements of the fluctuation amplitude on larger scales, particularly with those inferred from the microwave background anisotropies in the COBE 2-year data. By assuming a specific shape for the fluctuation spectrum, the COBE results may be extrapolated to $8h^{-1}\text{Mpc}$ and, in principle, comparison with equations (6.1) and (6.2) provides a test of the assumed spectral shape. This test, however, cannot yet be made completely rigorous because the available anisotropy data do not distinguish between contributions from scalar modes which determine the amplitude of the mass fluctuations, and contributions from tensor modes which produce gravitational waves. Furthermore, the asymptotic slope of the mass power spectrum, n , is poorly constrained by the anisotropy data and this introduces further uncertainty in the analysis of the COBE results (but not in the cluster abundance argument). As an illustration, we compare, in Fig 13, our estimates of σ_8 with the COBE values for the simplest possible

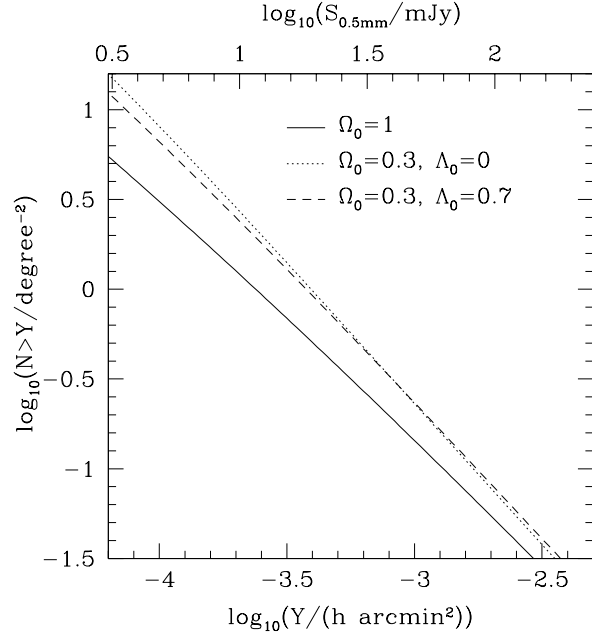


Figure 12. Sunyaev-Zel'dovich source counts as a function of Y for three different cosmologies. Solid lines correspond to $\Omega_0 = 1$, dotted lines to $\Omega_0 = 0.3$, and dashed lines to $\Omega_0 = 0.3, \Lambda_0 = 0.7$. The corresponding 0.5mm fluxes in mJy are shown on the top axis. About 60% more clusters with $Y > 10^{-3}h \text{ arcmin}^2$ are expected in the $\Omega_0 = 0.3$ models than in the $\Omega_0 = 1$ case.

case in which n takes the standard value of unity and tensor contributions are neglected. The hashed regions in the Figure show COBE estimates for $h = 0.8$ and $h = 0.5$, taken from Liddle *et al.* (1995a) in the open case, and from Liddle *et al.* (1995b) in the flat case. The dashed and solid lines give our estimates of σ_8 for the same two values of h , derived from the procedure described in Section 4, setting $\Gamma = \Omega_0 h \exp(-\Omega_b - \Omega_b/\Omega_0)$ (Sugiyama 1995) with the nucleosynthesis value of $\Omega_b = 0.013/h^2$ (Copi *et al.* 1995). Large values of h require low values of Ω_0 . Thus, if $h = 0.8$, Ω_0 is required to be less than 0.2, in the flat case, and less than 0.35 in the open case. If $h > 0.5$, values of $\Omega_0 \gtrsim 0.5$ are ruled out by this test whether or not $\Lambda_0 = 0$. For $\Omega_0 = 1$, $h = 0.27$ is required for consistency between COBE and the cluster abundances. Thus, as noted before by Efstathiou, Bond & White (1992) and White *et al.* (1993), the abundance of clusters in the standard CDM model ($h = 0.5$) is incompatible with the COBE fluctuations unless gravitational waves make a significant contribution to the measured microwave background anisotropies or there is a strong tilt in the primordial spectrum ($n \lesssim 0.8$; Bond 1995).

While the present day abundance of clusters may be used to determine the value of σ_8 with only a weak dependence on the power spectrum of fluctuations, the evolution of the cluster abundance may be used to set constraints on Ω_0 itself. These depend sensitively on the value of σ_8 and, to a lesser extent, on the shape of the fluctuation spectrum. In this study, we have, for the most part, restricted attention to models with spectral shape parameter, $\Gamma = 0.25$, consistent

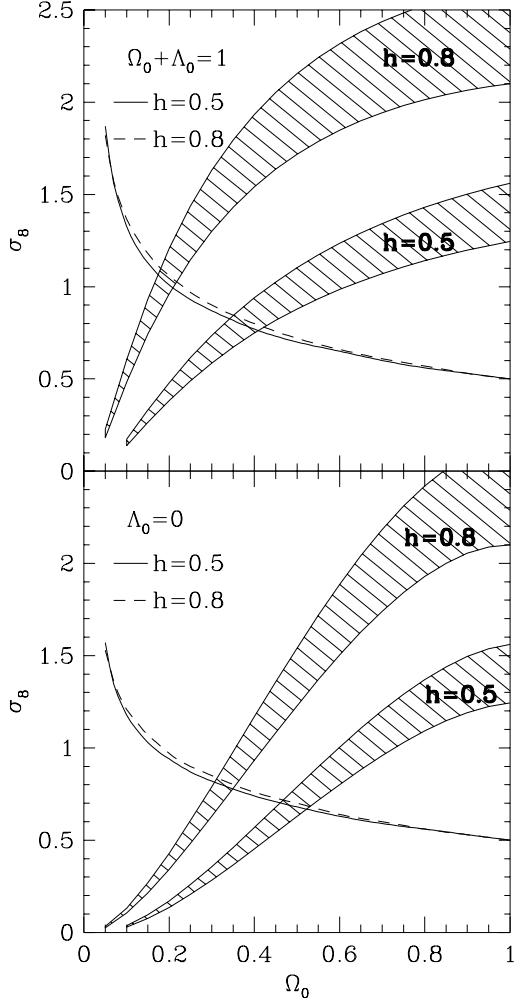


Figure 13. Comparison of σ_8 estimated from the COBE 2-year data and from the abundance of rich galaxy clusters. The top panel corresponds to flat models and the bottom panel to open models. The upper hatched region shows the COBE estimates for $h = 0.8$ and the lower hatched region the estimates for $h = 0.5$ as parameterised by Liddle *et al.* (1995a and b) with 12% errors in both cases. The dashed and solid lines show our estimates from the cluster abundance for $h = 0.8$ and $h = 0.5$ respectively, obtained through the procedure of Section 4, setting $\Gamma = \Omega_0 h \exp(-\Omega_b - \Omega_b/\Omega_0)$, where $\Omega_b = 0.013/h^2$ is the ratio of the mean baryon density to the critical density. The statistical errors in this case are less than 5%.

with observations of the large-scale distribution of galaxies (Efstathiou *et al.* 1992). Since the Ω_0 dependence of the evolutionary rate is so strong, the main effect of changing Γ is through its influence on the model normalization, σ_8 . However, as Figure 13 shows, this is a weak effect. Thus, in practice, this test of Ω_0 is insensitive to small departures from our assumed value of Γ . Furthermore, for interesting values of Ω_0 , the diagnostics we have considered depend only very weakly on Λ_0 . Thus, statistical studies of clusters at intermediate redshifts offer an excellent prospect for determining Ω_0 without the complications arising from the uncertain shape

of the galaxy power spectrum and the poorly understood relation between the distributions of galaxies and mass.

Different observables may be used to characterize the evolution of the cluster population. Here we have considered three properties for which observational data are likely to be obtained in the near future: the distribution of cluster masses, X-ray temperatures and S-Z decrements. The first may be derived from weak gravitational lensing studies; the second from existing and forthcoming X-ray surveys; and the last from ground-based observations and proposed space missions such as COBRA/SAMBA. Although the masses are perhaps the most difficult to measure, they provide a particularly robust test since, apart from the Press-Schechter ansatz, the only model assumption is the form of the density distribution of dark matter halos. In rough agreement with N-body simulations, we have taken this to be a singular isothermal sphere. In all cases, we have presented expected distributions at $z = 0.33$ and $z = 0.5$ and the predicted number counts of the largest clusters, both in space and in projection on the sky, as a function of redshift.

In agreement with previous analyses, we find that even at redshifts as low as 0.33, the comoving abundance of high mass or high X-ray temperature clusters is radically different in universes with $\Omega_0 = 1$ and $\Omega_0 = 0.3$. For example, at this redshift we expect 20 times as many clusters with $M > 3.5 \times 10^{14} h^{-1} M_\odot$ and 5 times as many clusters with $kT > 5$ keV if $\Omega_0 = 0.3$ than if $\Omega_0 = 1$. The corresponding factors at $z = 0.5$ are ~ 65 and 15. When integrating these cluster number densities with respect to redshift the effects of the different volume elements are included. Thus, the expected numbers of clusters per square degree on the sky out to redshift 0.5 differ by a factor of ~ 10 for both $M > 3.5 \times 10^{14} h^{-1} M_\odot$ and $kT > 5$ keV in these two cosmologies.

Whereas the mass and temperature functions only evolve dramatically if $\Omega_0 = 1$, the distribution of S-Z decrements (as measured by the Y -function of equation 2.10) declines rapidly with redshift in all cosmologies. This is mainly because, for the range of redshifts that we have considered, an object far away subtends a smaller angle on the sky than the same object placed nearby. Even so, at $z = 0.33$, the comoving number density of clusters with $Y = 10^{-3} h \text{ arcmin}^2$ is 10 times higher if $\Omega_0 = 0.3$ than if $\Omega_0 = 1$. However, the overall abundances at this redshift are all very low because of the rapid decrease in the angular size of the clusters with redshift. The projected counts are dominated by low redshift clusters and, as a result, the expected excess of clusters with $Y > 10^{-3} h \text{ arcmin}^2$ is only $\sim 60\%$ if $\Omega_0 = 0.3$. This excess becomes larger as the Y threshold is lowered and higher redshift clusters are included.

To obtain an estimate of Ω_0 using any of the tests proposed in this paper requires complete samples of intermediate redshift clusters selected according to the statistic under consideration. Samples of S-Z clusters are likely to be Y -limited in any case. For the other diagnostics, selecting by X-ray luminosity is probably an efficient method. Since X-ray luminosity correlates reasonably well with X-ray temperature (at least locally) and, apparently also with lensing mass (Smail *et al.* 1996), the sample completeness with respect to the relevant statistic may be determined *a posteriori* from these data. Incomplete datasets, on the other hand, may be used to set *upper limits* on Ω_0 because the abundance

of clusters at intermediate redshift declines monotonically with increasing Ω_0 .

There are already several X-ray bright clusters known at high redshift. For example, Luppino & Gioia (1995) report the detection of 6 such clusters with $z = 0.5$ in the EMSS survey (Henry *et al.* 1992). Measurements of their X-ray temperatures would be extremely valuable. They might confirm the indication from velocity dispersion measurements that these clusters are hot, suggesting that Ω_0 is low, or they might show that these velocity dispersions are overestimated as a result of contamination by projection effects. The lowest velocity dispersion reported for these clusters corresponds to a temperature of 6.6 keV. As an illustration, if we assume that the effective area surveyed to find these six clusters was 200 square degrees, then we would expect to find < 0.04 clusters above this temperature if $\Omega_0 = 1$; ~ 6 if $\Omega_0 = 0.3$ and $\Lambda_0 = 0.7$; and ~ 30 if $\Omega_0 = 0.3$ and $\Lambda_0 = 0$. However, if the coolest of these clusters actually has a temperature of only 3 keV, then we would have expected ~ 30 examples even if $\Omega_0 = 1$.

In summary, a statistical sample of X-ray clusters at intermediate redshifts with measured temperatures or S-Z decrements could place a strong constraint on the density parameter Ω_0 .

ACKNOWLEDGMENTS

We thank Hugh Couchman for providing a copy of his excellent AP³M N-body code and for giving valuable advice and support. We thank David Weinberg for generously allowing us first use of this set of N-body simulations and Pat Henry for his helpful advice and comments on the manuscript. VRE acknowledges support of a PPARC studentship and SMC of a PPARC Advanced Fellowship. This work was also supported by a PPARC rolling grant.

REFERENCES

- Bahcall, N.A., Cen, R., 1993. ApJ, 407, L49.
 Barbosa, D., Bartlett, J.G., Blanchard, A., Oukbir, J., 1995. A&A, submitted. (astro-ph 9511084)
 Bartlett, J.G., Silk, J., 1993. ApJ, 407, L45.
 Bartlett, J.G., Silk, J., 1994. ApJ, 423, 12.
 Birkinshaw, M., Hughes, J.P., 1994. ApJ, 420, 33.
 Bond, J.R., Cole, S., Efstathiou, G., Kaiser, N., 1991. ApJ, 379, 440.
 Bond, J.R., Myers, S.T., 1993. In NASA. Ames Research Center, The Evolution of Galaxies and Their Environment, p52-53.
 Bond, J.R., 1995. To be published in *The Evolution of the Universe*, Dahlem Workshop Report ES19. (astro-ph 9512142)
 Bryan, G.L., Cen, R., Norman, M.L., Ostriker, J.P., Stone, J.M., 1994. ApJ, 428, 405.
 Cen, R.Y., Ostriker, J.P., 1994. ApJ, 429, 4.
 Cole, S., Lacey, C., MNRAS, submitted. (astro-ph 9510147)
 Copi C.J., Schramm D.N., Turner M.S., 1995. Science, 267, 192.
 Couchman, H.M.P., 1991. ApJ.Lett, 368, 23.
 Davis, M., Efstathiou, G., Frenk, C.S., White, S.D.M., 1985. ApJ, 292, 371.
 Edge, A.C., 1988. Thesis, University of Leicester.
 Edge, A.C., Stewart, G.C., Fabian, A.C., Arnaud, K.A., 1990. MNRAS, 245, 559.
 Efstathiou, G., Bond, J.R., White, S.D.M., 1992. MNRAS, 258, 1P.
 Evrard, A.E., 1989. ApJ, 341, L71.
 Evrard, A.E., 1990. ApJ, 363, 349.
 Evrard, A.E., Metzler, C.A., Navarro, J.F., 1995. ApJ, submitted. (astro-ph 9510058)
 Fahlman, G., Kaiser, N., Squires, G., Woods, D., 1994. ApJ, 437, 56.
 Forman, W.F., Jones, C.J., 1990. In *Clusters of Galaxies*, eds Oegerle, W.R., Fitchett, M.J., Danly, L., page 257, CUP.
 Frenk, C.S., White, S.D.M., Efstathiou, G., Davis, M., 1990. ApJ, 351, 10.
 Girardi, M., Biviano, A., Giuricin, G., Mardirosian, F., Mezzetti, M., 1993. ApJ, 404, 38.
 Grainge, K., Jones, M., Pooley, G., Saunders, R., Edge, A., 1993. MNRAS, 265, L57.
 van Haarlem, M.P., Frenk, C.S., White, S.D.M., 1996. MNRAS, submitted.
 Hanami, H., 1993. ApJ, 415, 42.
 Hattori, M., Matsuzawa, H., 1995. A&A, 300, 637.
 Henry, J.P., Arnaud, K.A., 1991. ApJ, 372, 410.
 Henry, J.P., Gioia, I.M., Maccacaro, T., Morris, S.L., Stocke, J.T., Wolter, A., 1992. ApJ, 386, 408.
 Kaiser, N., Squires, G., 1993. ApJ, 404, 441.
 Kochanek, C.S., 1995. ApJ, 453, 545.
 Lacey C., Cole S., 1993. MNRAS, 262, 627.
 Lacey C., Cole S., 1994. MNRAS, 271, 676.
 Lahav, O., Lilje, P.B., Primack, J.R., Rees, M.J., 1991. MNRAS, 251, 128.
 Liddle, A.R., Lyth, D.H., Roberts, D., Viana, P.T.P., 1995a. MNRAS submitted. (astro-ph 9506091)
 Liddle, A.R., Lyth, D.H., Viana, P.T.P., White, M., 1995b. MNRAS submitted. (astro-ph 9512102)
 Lilje, P.B., 1992. ApJ, 386, L33.
 Luppino, G.A., Gioia, I.M., 1995. ApJ.Lett, in press.
 Maoz, E., 1990. ApJ, 359, 257.
 Maddox, S.J., Efstathiou, G., Sutherland, W.J., Loveday, J., 1990. MNRAS, 242, 43P.
 Maddox, S.J., Efstathiou, G., Sutherland, W.J., 1996. MNRAS submitted.
 Markevitch, M., Mushotzky, R., Inoue, H., Yamashita, K., Furuzawa, A., Tawara, Y., 1996. ApJ, 456, 437.
 Mather, J. C., *et al.*, 1994, ApJ, 420,439.
 Mazure, A., *et al.*, 1995. A & A, accepted. (astro-ph 9511052)
 Navarro, J.F., Frenk, C.S., White, S.D.M., 1995. MNRAS, 275, 720.
 Oukbir, J., Blanchard, A., 1992. A&A, 262, L21.
 Peebles P.J.E., 1980. The Large Scale Structure of the Universe. Princeton Univ. Press, Princeton, NJ
 Peebles P.J.E., 1984. ApJ, 284, 439.
 Press W.H., Schechter P., 1974. ApJ, 187, 425.
 Seitz, C., Schneider, P., 1995. A&A, 297, 287.
 Smail, I., Ellis, R.S., Dressler, A., Couch, W.J., Oemler, A., Butcher, H., Sharples, R.M., 1996. ApJ, submitted.
 Sugiyama N., 1995. ApJS, 100, 281.
 Sunyaev, R.A., Zel'dovich Ya. B., 1972. Comm. Astrophys. Space Phys. 4,173
 Tsai, J.C., Katz, N., Bertschinger, E., 1994. ApJ, 423, 553.
 Viana, P.T.P., Liddle, A.R., MNRAS, submitted. (astro-ph 9511007)
 White S.D.M., Efstathiou G., Frenk C.S., 1993. MNRAS, 262, 1023.
 Wilbanks, T.M., Ade, P.A.R., Fischer, M.L., Holzappel, W.L., Lange, A.E., 1994. ApJ, 427, L75.
 Wilson, G., Cole, S., Frenk, C.S., 1996. MNRAS, in press.
 Zabludoff, A.I., Huchra, J.P., Geller, M.J., 1990. ApJS, 74, 1.

APPENDIX A: THE SPHERICAL COLLAPSE MODEL FOR $\Omega + \Lambda = 1$

It can be shown (Peebles 1984) that the variation of the radius, r , of a uniform spherical overdensity with scale factor a is described, for a flat cosmology with a cosmological constant, by

$$\left(\frac{dr}{da}\right)^2 = \frac{r^{-1} + \omega r^2 - \kappa}{a^{-1} + \omega a^2}, \quad (\text{A1})$$

where $a = (1+z)^{-1}$, κ is a constant which for overdensities takes positive values and

$$\omega = (\Omega_0^{-1} - 1). \quad (\text{A2})$$

Therefore a perturbed region will turnaround when

$$\omega r^3 - \kappa r + 1 = 0. \quad (\text{A3})$$

Solving this cubic and requiring that a physically sensible root exists we find the smallest perturbation which will collapse has

$$\kappa_{\min} = \frac{3\omega^{\frac{1}{3}}}{2^{\frac{2}{3}}}. \quad (\text{A4})$$

The corresponding turnaround radius is

$$r_{\text{ta,max}} = (2\omega)^{-\frac{1}{3}}. \quad (\text{A5})$$

Perturbations with larger values of κ turnaround and collapse earlier. Solving the cubic (A3) we find the turnaround radius r_{ta} as a function of the density parameter ω and perturbation amplitude κ . The solution can be expressed as

$$r_{\text{ta}} = -2s^{\frac{1}{3}} \cos\left(\frac{\theta}{3} - \frac{2\pi}{3}\right), \quad (\text{A6})$$

where

$$s = \left(\frac{3}{2}\right)^3 \left(\frac{\kappa}{\kappa_{\min}^3}\right)^{\frac{3}{2}} \quad (\text{A7})$$

and θ satisfies

$$\cos\theta = \left(\frac{\kappa_{\min}}{\kappa}\right)^{\frac{3}{2}} \quad \left(0 < \theta < \frac{\pi}{2}\right). \quad (\text{A8})$$

In order to calculate the redshifts corresponding to turnaround and collapse we separate the variables in (A1) and integrate,

$$\int_0^{r_{\text{ta}}} \frac{r^{\frac{1}{2}}}{(\omega r^3 - \kappa r + 1)^{\frac{1}{2}}} dr = \int_0^{a_{\text{ta}}} \frac{a^{\frac{1}{2}}}{(\omega a^3 + 1)^{\frac{1}{2}}} da. \quad (\text{A9})$$

Defining

$$I(\omega, \kappa) = \int_0^{r_{\text{ta}}} \frac{r^{\frac{1}{2}}}{(\omega r^3 - \kappa r + 1)^{\frac{1}{2}}} dr, \quad (\text{A10})$$

which must be evaluated numerically, the expansion factor at turnaround, a_{ta} , and at collapse, a_c , satisfy the implicit equations,

$$I(\omega, \kappa) = \int_0^{a_{\text{ta}}} \frac{a^{\frac{1}{2}}}{(\omega a^3 + 1)^{\frac{1}{2}}} da \quad (\text{A11})$$

and

$$2I(\omega, \kappa) = \int_0^{a_c} \frac{a^{\frac{1}{2}}}{(\omega a^3 + 1)^{\frac{1}{2}}} da, \quad (\text{A12})$$

where the collapse time is defined in the usual way to be that at which (A1) predicts collapse to a point singularity. Using the substitution $u = \sqrt{\omega a^3}$, these equations can be integrated analytically to give

$$a_{\text{ta}} = \left[\frac{\exp(3\sqrt{\omega}I(\omega, \kappa)) - 1}{2\sqrt{\omega}} \right]^{\frac{2}{3}} \exp(-\sqrt{\omega}I(\omega, \kappa)) \quad (\text{A13})$$

and

$$a_c = \left[\frac{\exp(6\sqrt{\omega}I(\omega, \kappa)) - 1}{2\sqrt{\omega}} \right]^{\frac{2}{3}} \exp(-2\sqrt{\omega}I(\omega, \kappa)) \quad (\text{A14})$$

Hence we have a_c , or equivalently z_c , the redshift of collapse of a spherical overdensity, as a function of ω and κ .

To calculate Δ_c , the density of virialised object in terms of critical density, we make use of the expression from (Lahav *et al.* 1991) which gives the ratio between the radius of the virialised sphere and its turnaround radius. Given the expression above for the turnaround radius and the expansion factor at collapse, Δ_c is given by

$$\Delta_c = \Omega(a_c) \left(\frac{a_c}{r_c}\right)^3. \quad (\text{A15})$$

All that remains is to relate κ to the quantity more often used to describe a perturbation, namely δ_0 , the linear theory overdensity extrapolated to the present. This in turn is related to the linear theory overdensity at collapse, δ_c , by

$$\delta_c = \delta_0 D(a_c) \quad (\text{A16})$$

where $D(a)$ represents the linear theory growth factor normalised to unity at the present, $D(a_0) = 1$. For the $\Omega_0 + \Lambda_0 = 1$, $\Omega_0 < 1$ case

$$D(a) = \frac{A(a(2\omega)^{1/3})}{A(a_0(2\omega)^{1/3})}, \quad (\text{A17})$$

where

$$A(x) = \frac{(x^3 + 2)^{\frac{1}{2}}}{x^{\frac{3}{2}}} \int^x \left(\frac{u}{u^3 + 2}\right)^{\frac{3}{2}} du \quad (\text{A18})$$

(Peebles 1980). In the limit where $a \ll 1$ we find

$$\delta = \frac{\delta_0 a_0 (2\omega)^{1/3}}{5A(a_0(2\omega)^{1/3})} a + O(a^2), \quad (\text{A19})$$

which can be compared to the corresponding expression

$$\delta = \frac{3\kappa}{5} a + O(a^2), \quad (\text{A20})$$

derived from (A1). Identifying terms we find

$$\kappa = \frac{a_0(2\omega)^{1/3}}{3A(a_0(2\omega)^{1/3})} \delta_0. \quad (\text{A21})$$

Now given the density parameter Ω_0 and the amplitude of a density perturbation, δ_0 we can compute ω using (A2) and κ using (A21). Then the collapse redshift can be obtained from (A6), (A10) and (A14). The corresponding values of δ_c and Δ_c are then given by (A16) and (A15). The dashed lines in Figure 1 show δ_c and Δ_c as functions of Ω at the time of collapse.